

Surface plasmon driven lowering of the electron emission order in a carbon/gold bilayer film

S. R. Greig, A. Morteza-Najarian, R. L. McCreery, and A. Y. Elezzabi

Citation: [Applied Physics Letters](#) **109**, 221104 (2016); doi: 10.1063/1.4969066

View online: <http://dx.doi.org/10.1063/1.4969066>

View Table of Contents: <http://scitation.aip.org/content/aip/journal/apl/109/22?ver=pdfcov>

Published by the [AIP Publishing](#)

Articles you may be interested in

[An ultrafast nanotip electron gun triggered by grating-coupled surface plasmons](#)

Appl. Phys. Lett. **107**, 231105 (2015); 10.1063/1.4937121

[Electrical stability enhancement of the amorphous In-Ga-Zn-O thin film transistor by formation of Au nanoparticles on the back-channel surface](#)

Appl. Phys. Lett. **102**, 102108 (2013); 10.1063/1.4795536

[Enhanced H₂S response of Au modified Fe₂O₃ thin films](#)

AIP Conf. Proc. **1512**, 782 (2013); 10.1063/1.4791271

[Surface-plasmon-enhanced band-edge emission from Au/GaN powders](#)

Appl. Phys. Lett. **98**, 161906 (2011); 10.1063/1.3581214

[Ponderomotive electron acceleration using surface plasmon waves excited with femtosecond laser pulses](#)

Appl. Phys. Lett. **86**, 264102 (2005); 10.1063/1.1946202

The advertisement features the Lake Shore Cryotronics logo on the left, which includes a blue square icon and the text 'Lake Shore CRYOTRONICS'. In the center is a photograph of a large, industrial-grade cryogenic measurement system, the NEW 8600 Series VSM, with a computer monitor and various sensors. On the right, the text reads 'NEW 8600 Series VSM' in large orange letters, followed by 'For fast, highly sensitive measurement performance' in white. At the bottom right, there is a 'LEARN MORE' button with a right-pointing arrow.

Surface plasmon driven lowering of the electron emission order in a carbon/gold bilayer film

S. R. Greig,^{1,a)} A. Morteza-Najarian,^{2,3} R. L. McCreery,^{2,3} and A. Y. Elezzabi¹

¹Ultrafast Optics and Nanophotonics Laboratory, Department of Electrical and Computer Engineering, University of Alberta, Edmonton, Alberta T6G 1H9, Canada

²National Institute for Nanotechnology, National Research Council, Edmonton, Alberta T6G 2M9, Canada

³Department of Chemistry, University of Alberta, Edmonton, Alberta T6G 2G2, Canada

(Received 23 August 2016; accepted 15 November 2016; published online 29 November 2016)

We demonstrate the reduction of the nonlinear surface plasmon driven electron emission order from a bilayer of electron beam evaporated carbon (eC) and gold (Au). Higher confined electric fields, and the presence of sp^2/sp^3 clustering in the eC layer increase the electron emission at lower orders via field-driven energy gain. This bilayer provides a platform for ultrafast surface plasmon driven electron sources. *Published by AIP Publishing.* [<http://dx.doi.org/10.1063/1.4969066>]

Recently there has been a great interest in the generation of ultrashort, high energy electron pulses via surface plasmon (SP) waves excited by ultrafast lasers.^{1–3} SP based sources can achieve shorter pulse durations, and can be made more compact compared to direct laser-driven electron sources. As well, multiple geometries can be used to excite the necessary SP waves including prisms,^{3–6} nanoantennas,^{7,8} nanotips,^{9,10} and gratings.¹¹ The main operating principle is the release of free electrons from a metallic film, followed by the subsequent SP field-driven acceleration to high energies. This technique has previously been used to generate high energy, femtosecond electron pulses.³ However, a major issue facing SP based electron pulse generation at low intensities is the number of photons required to free an electron from the potential barrier at the surface, i.e., the metal's work function, W_F . Typically, $\lambda = 800$ nm ultrashort laser pulses from Ti:sapphire lasers are used to excite the SP waves and consequently to generate electrons from either Au or Ag films. Based on the work function of these metals, this requires absorption of multiple photons by an electron to overcome W_F and be released into vacuum, where it can interact with the SP field. As this absorption process is highly nonlinear, and thus requires high laser intensities, it is advantageous to reduce the number of photons required. The metal-vacuum interface barrier, and thus the number of required photons, can be lowered through the application of a DC extraction voltage. A similar effect can be achieved by increasing the incident laser light intensity such that the barrier is lowered enough to allow for single photon tunnel ionization.^{4–6} However, achieving these high laser light intensities ($\sim 10^{12}$ W/cm²) necessitates the use of complex high powered laser amplifier systems to reach the strong-field laser-matter interaction regime.^{4,12} Nonetheless, there is an upper limit to which the laser light intensity, or DC voltage can be increased, namely, the laser induced damage threshold and the DC electric field breakdown of the materials involved. Therefore, it is of paramount importance to reduce the order of the nonlinearity involved while utilizing low laser light intensities.

To achieve this, one requires an alternative source of electrons that acts in unison with the plasmonic metal. As such, a nonmetallic material can be introduced that acts as a source/reservoir of electrons. However, there are two issues that need to be addressed using this approach: a nonmetallic/metallic surface interface can introduce an inversion/depletion region that can impede the flow of electrons into the metal layer; and the nonmetallic material can interfere with the coupling and propagation of the SP at the metal-vacuum interface. This limits the choices of nonmetallic materials to dielectrics with low absorption so as not to disturb the SP field at the metal-vacuum interface and whose fermi level lines up exactly with that of the metal.

In this letter, we show the reduction of the nonlinear electron emission order of an ultrafast SP based electron source through the use of a nonmetallic/metallic bilayer film. By introducing a thin layer of electron beam evaporated carbon (eCarbon or eC) to act as a reservoir of electrons underneath an Au film, the electron emission order is reduced when compared to an Au film by itself. Furthermore, we show that the eC layer does not perturb the SP coupling, or the electromagnetic fields at the Au-vacuum interface necessary for electron acceleration.

Laser pulses having a central wavelength of 800 nm and a pulse duration of 15 fs from a Ti:sapphire laser oscillator with a repetition rate of 76 MHz were focused to a 70 μ m spot size to excite SP waves on Au metal films in the Kretschmann geometry ([supplementary material](#)). The first sample consists of a 45 nm Au film deposited on a UV fused silica prism, while the second sample has a 10 nm layer of eC underneath the 45 nm Au film. The Au and the eC films are deposited via electron beam evaporation at 0.03 nm/s for Au and <0.01 nm/s for eC, using targets of pure Au and spectroscopic graphite rods (SPI Supplies, PA). eCarbon is amorphous and contains approximately 30% sp^3 hybridized carbon, with the remainder sp^2 (Ref. 13). The prisms are placed in a vacuum chamber, at a pressure of $\sim 10^{-5}$ Torr, and photocurrent from each sample, when illuminated by the 800 nm laser pulses, is detected with a channeltron electron multiplier connected to a lock-in amplifier.

Figure 1(a) depicts the ultraviolet photoemission spectroscopy (UPS) spectra for a 10 nm eC film, a 20 nm Au film,

^{a)}Electronic mail: sgreig@ualberta.ca

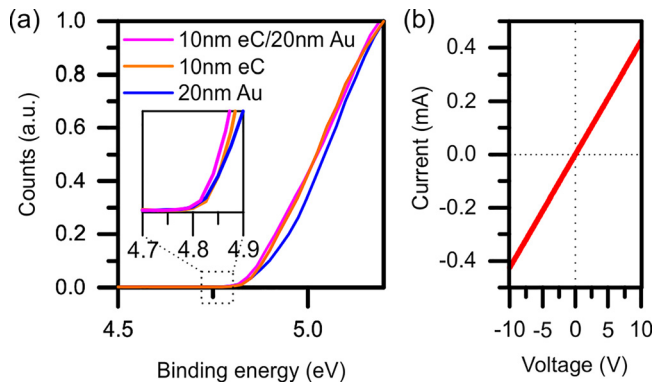


FIG. 1. (a) Measured ultraviolet photoemission spectroscopy spectra for a 10nm eC film, a 20nm Au film, and a 10nm eC film beneath a 20nm Au film, indicating a 4.8 eV work function for eC and Au alone, and the eC/Au bilayer. (b) Four-point current vs. voltage measurement indicating the absence of a built-in field at the eC/Au interface.

and a eC/Au bilayer film. The onset of electron photoemission from all three films arises at 4.8 eV (inset of Fig. 1(a)), indicating that the Au, eC, and eC/Au films have the same work function of 4.8 eV. The linear behavior of a four-point current-voltage electrical measurement, shown in Fig. 1(b), of the eC/Au contact junction indicates the absence of a built-in field at the eC/Au interface.¹⁴ When modifying a plasmonic structure, it is of great importance to not disturb the SP coupling behavior. Figure 2 shows the measured reflected laser pulse spectrum at the SP resonance of each film, indicating a similar broadband SP coupling for both the Au and eC/Au films. At the SP resonance only 8%–10% of the incident light is reflected. It should be noted that the spectra are normalized, as such their counts cannot be directly compared. The black curve illustrates the spectrum of the laser pulse reflected off an Au mirror. Furthermore, based on the finite-difference time-domain (FDTD) simulations performed, the SP electric fields at the Au-vacuum interface are within 5% of each other for each sample. A cut of the laser electric field squared, $|E|^2$, along a direction normal to the surface of the films, determined by FDTD simulations, is depicted in Figs. 3(a) and 3(b) for the Au layer by itself and the eC/Au bilayer, respectively. The material parameters for eC and Au were determined by spectroscopic ellipsometry. Clearly, the introduction of the thin eC layer does not alter the SP coupling.

A strong optical field incident on a metal surface can free electrons from the surface through a nonlinear process.

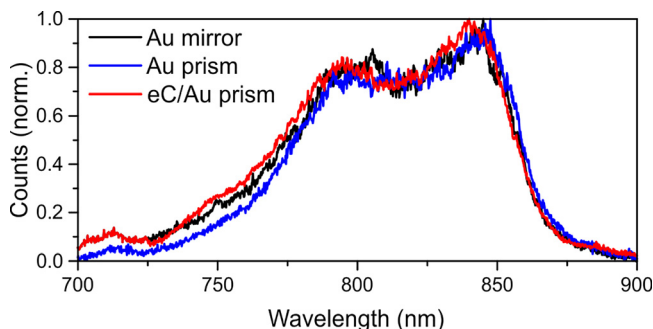


FIG. 2. Spectrum of reflected laser pulse from Au and eC/Au films at the SP resonance. The black curve shows the spectrum of the laser pulse reflected off an Au mirror. Note that the counts are normalized.

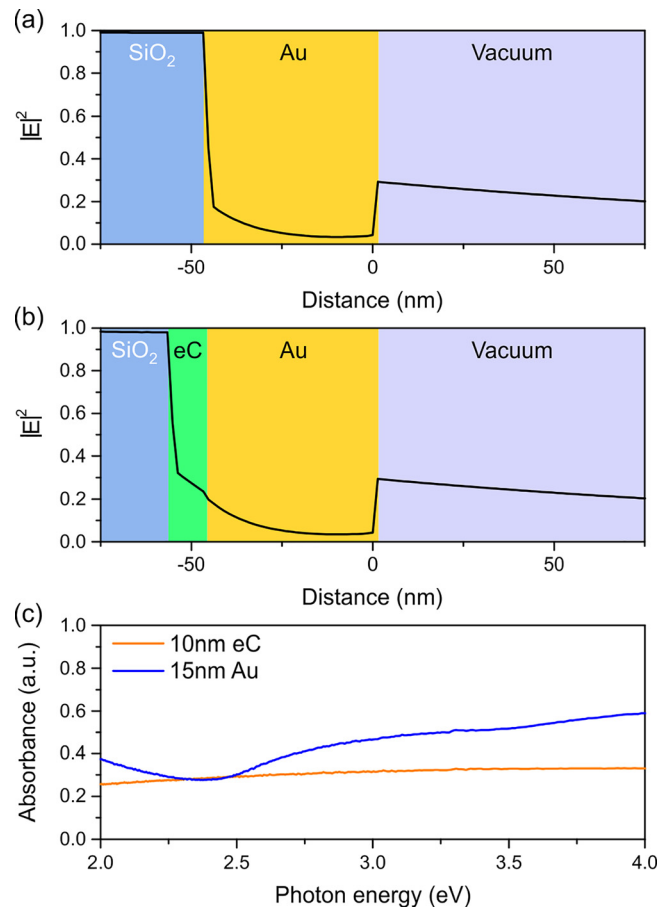


FIG. 3. Cut of the laser electric field squared from FDTD simulations along a direction normal to the film for (a) Au and (b) eC/Au films. (c) Measured absorbance for a 10 nm eC film and a 15 nm Au film.

At a certain intensity, the photoemission process crosses from the multi-photon ionization regime to the tunnel ionization regime. This crossover point is typically found to occur when the Keldysh parameter, $\gamma = \omega \sqrt{(2m_e W_F)} / (qE_{laser})$, equals 1, here ω is the angular frequency of the laser, m_e is the electron mass, q is the elementary electric charge, and E_{laser} is the incident laser electric field. For $\gamma > 1$, the emission will be a multi-photon absorption process, while $\gamma < 1$ indicates a tunnel ionization process. Within the tunnel ionization regime, the number of photons required can be lowered to only a single photon.

Exciting the SP at a low laser intensity ($< 9.9 \text{ GW/cm}^2$ (Ref. 4)) such that the emission process is occurring fully within the multi-photon absorption regime provides a platform to study the effect of the eC/Au bilayer on the number of photons required to free an electron. Based on the work function of 4.8 eV for Au and eC (see inset of Fig. 1(a)), and with each photon possessing an energy of ~ 1.4 – 1.7 eV, freeing an electron from an Au or an eC/Au film requires a minimum of a three-photon absorption (3PA) process to take place. At the laser intensities used here, the Keldysh parameter is calculated to be $\gamma = 21$ at the lowest intensity of 0.37 GW/cm^2 , and $\gamma = 11$ at 1.35 GW/cm^2 , with a surface electric field enhancement of 21 times.⁵ To experimentally verify the electron emission order, the incident laser intensity was varied between 0.37 GW/cm^2 and 1.35 GW/cm^2 . By operating with a maximum intensity of 1.35 GW/cm^2 , thermal

effects within the metallic films are avoided.¹⁵ The measured photocurrent, J , for the Au and the eC/Au samples, as a function of laser intensity, I_{laser} , are depicted in Figs. 4(a) and 4(b), respectively. A slope of $n = 3.01 \pm 0.05$ is found for the Au sample, and a slope of $n = 2.44 \pm 0.03$ is found for the eC/Au sample. In an ideal multiphoton absorption photoemission process, one would expect the order, n , to be an integer number corresponding to the power dependence of the measured photocurrent, i.e., $J \propto I_{laser}^n$. While the $n = 3$ is expected for the Au film (Fig. 5), the $n = 2.44$ for the eC/Au bilayer suggests that electrons must be originating from another, lower order emission process. However, the work function of eC is measured to be identical to that of Au, i.e., 4.8 eV. As such, any electron released would require the absorption of at least three photons, i.e., $n = 3$. Examining the absorbance of a 10 nm eC film, and a 15 nm Au film over the ultraviolet-visible wavelength range (Fig. 3(c)), shows a broadband absorption in eC, indicating many possible local optical transitions between a range of states present in the disordered carbon matrix.¹⁶ In addition, the absence of any strong absorption peaks indicates that there is no direct two-photon ionization of the eC layer. Evidently, the electron emission for the eC/Au sample must be originating from the absorption processes of different orders with different probabilities.

To discern the low order of the photoemission process, one needs to examine the electrons in the presence of the SP field. It is well known that in the presence of high electric fields, the vacuum potential barrier, ϕ , can be lowered via the Schottky effect.^{14,17} The potential barrier under influence of an electric field is given by:¹⁴ $\phi(x) = W_F - q^2/16\pi\epsilon_0x - qE_{laser}x$, where ϵ_0 is the permittivity of free space, and x is the distance from the interface into the vacuum. In the above measurements, at the lowest incident field of $E_{laser} = 5.3 \times 10^5$ V/cm (or $I_{laser} = 0.37$ GW/cm²), and at an average SP electric field enhancement of 21 times, ϕ is lowered by 1.1 eV to $\phi_l = 3.7$ eV. However, the value of ϕ_l is not low enough to allow for a reduction in the electron emission order. Additionally, if ϕ_l was low enough, the reduction would be observed for both samples. Therefore, there must be another mechanism responsible for the observed $n = 2.44$ in the eC/Au sample.

Just as electrons are accelerated in the SP field present at the Au-vacuum interface,³⁻⁵ electrons are also accelerated

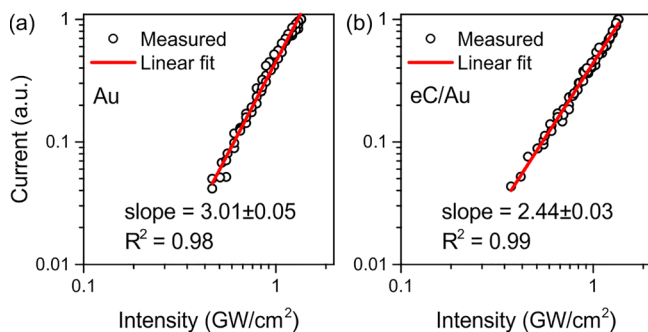


FIG. 4. Measured current as a function of incident laser intensity indicating (a) three-photon ionization in the Au sample, and (b) a combination of absorption processes of different orders with different probabilities in the eC/Au sample.

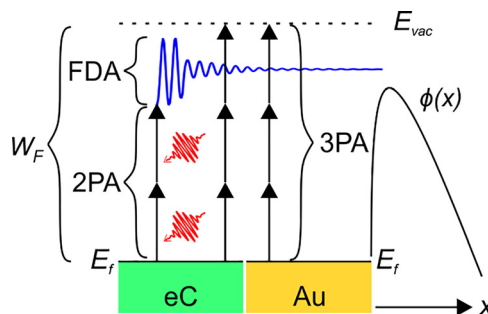


FIG. 5. Energy band diagram at the eC/Au interface representing the two emission processes; two-photon absorption (2PA) followed by field-driven acceleration (FDA) and emission over the lowered ϕ ; and direct three-photon absorption (3PA). Each arrow represents a single photon with 1.6 eV energy. E_f is the fermi level, E_{vac} is the vacuum energy level, and x is directed away from the Au-vacuum interface.

by the electric fields within the materials themselves.¹⁸ Consider electrons that are generated by one-photon absorption (1PA) and two-photon absorption (2PA), resulting in initial energies of 1.6 eV and 3.2 eV, respectively. The electrons are then subsequently accelerated (decelerated) to higher (lower) kinetic energies by the electric fields present within the materials. Clearly, at the electric fields here, one-photon generated electrons will not be able to gain enough energy to overcome ϕ_l and thus cannot contribute to J . On the contrary, for 2PA generated electrons, the minimal kinetic energy gain is quite achievable to overcome ϕ_l . Figure 5 illustrates the field-driven acceleration of 2PA generated electrons over ϕ_l .

To verify that the kinetic energy of the field-accelerated electrons is enough to overcome ϕ_l , particle tracking simulations are performed with electromagnetic fields calculated from FDTD simulations. The simulation methodology is described in detail elsewhere.^{1,19} Briefly, electrons are tracked in time and space as they interact with the electric and magnetic fields of the incident laser pulse and surface plasmon. Each electron is given an initial kinetic energy in the range of 2.8–3.4 eV, corresponding to 2PA of the laser pulse. Figure 6(a) depicts the kinetic energy of $n = 2$ generated electrons at the Au-vacuum interface for the Au sample at three incident intensities (0.37, 0.85, and 1.35 GW/cm²). The quasi-symmetric shape of the kinetic energy spread can be ascribed to the fact that the acceleration process is highly dependent on the phase of the SP field when the electron is generated. As such, a similar number of electrons that are accelerated will be decelerated. At the lowest electric field of 5.3×10^5 V/cm, (i.e., $I_{laser} = 0.37$ GW/cm²), no electron is able to gain enough kinetic energy to overcome ϕ_l . As the electric field strength increases, the barrier continues to lower, and the electrons will gain enough kinetic energy to overcome the lowered barrier at the Au-vacuum interface. At $E_{laser} = 8 \times 10^5$ V/cm (i.e., $I_{laser} = 0.85$ GW/cm²) only 2% of 2PA generated electrons will have enough energy to overcome the $\phi_l = 3.45$ eV barrier, this increases to 19% at $E_{laser} = 1 \times 10^6$ V/cm (i.e., $I_{laser} = 1.35$ GW/cm²) for the $\phi_l = 3.3$ eV barrier. Due to the low number of $n = 2$ generated electrons reaching the vacuum, the normal $n = 3$ absorption process will completely dominate the emission process and result in the observed order of $n = 3.01$.

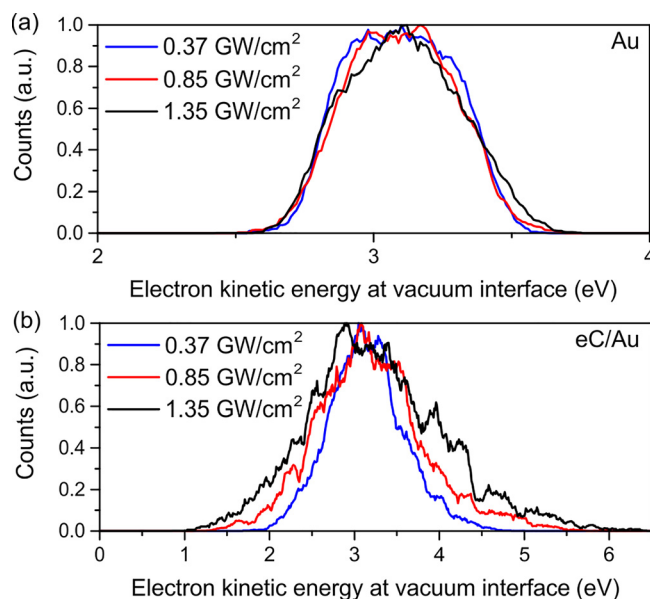


FIG. 6. Simulated electron kinetic energy spectra at the Au-vacuum interface at various incident laser intensities for the (a) Au layer by itself, and (b) eC/Au bilayer. The electrons are given an initial kinetic energy in the range of 2.8–3.4 eV, corresponding to an electron generated by two-photon absorption of the incident laser pulse. The eC/Au spectrum is broader than the Au spectrum due to the higher accelerating SP field in the eC layer. Note that all electron counts are normalized, and there is a difference in energy scales between (a) and (b).

On the contrary, for the eC/Au sample, even with the 10 nm eC layer, the situation is different. First, there is a significant increase in electric field strength within the eC layer compared to the Au layer. Calculating the average $|E|$ obtained from FDTD simulations in each layer indicates 2.2 times higher average $|E|$ in the eC layer of the eC/Au sample compared to the Au sample. Second, the effective mass of electrons within eC is 78% of the effective mass in Au. Therefore, at a given E_{laser} , the relative acceleration, a_{rel} , experienced by an electron in eC compared to an electron in Au will be higher. The relative acceleration is given by $a_{rel} = \eta m_{Au}/m_{eC}$, where $m_{Au} = 1.12$ is the electron effective mass in Au,²⁰ $m_{eC} = 0.87$ is the electron effective mass in eC,²¹ and $\eta = 2.2$ is the aforementioned ratio of electric fields between the eC film and Au film. This results in 2.8 times higher electron acceleration in the eC film compared to that in the Au film. Furthermore, in addition to the electric field enhancement from the SP, there is also field enhancement from the composition of the eC film itself. It is well known that for field emission from carbon films, the nano-clusters of conductive, graphitic, sp^2 bonds embedded in insulating, diamond-like, sp^3 bonds lead to increased localized electric field enhancement within the carbon.^{22–25} It is possible that at the interface between eC and Au, sp^3 bonds are converted into sp^2 bonds,²⁶ resulting in further increase of sp^2 clustering directly at the interface, and hence, an increase in the electric field enhancement at the eC/Au interface. At an SP electric field enhancement of 21 times, combined with an eC electric field enhancement of 56 times,²² 2PA generated electrons from the eC can gain enough kinetic energy to be emitted over ϕ_l . Note that ϕ will only be lowered due to the SP field enhancement directly at the Au-vacuum interface, and will not be affected by the localized

sp^2/sp^3 clustering field enhancement. Figure 6(b) depicts the kinetic energy of $n=2$ accelerated electrons at the Au-vacuum interface at various incident laser intensities. Notably, at the lowest electric field of 5.3×10^5 V/cm, (i.e., $I_{laser} = 0.37$ GW/cm²), 11% of the electrons possess enough kinetic energy to overcome the barrier. This increases to 33% at $E_{laser} = 8 \times 10^5$ V/cm (i.e., $I_{laser} = 0.85$ GW/cm²) and 45% at $E_{laser} = 1 \times 10^6$ V/cm (i.e., $I_{laser} = 1.35$ GW/cm²). Note that the model used does not take into account the local density of states of the eC. As such, the percentages do not correspond directly to an absolute number of electrons. Evidently, approximately half of the 2PA generated electrons originating from the eC layer will be emitted from the sample. Given that an $n=2$ absorption process has a higher probability of occurring than an $n=3$ absorption process, it can be concluded that the $n=2$ accelerated electrons dominate the observed current, as exhibited by the lowering of the emission order to $n = 2.44$.

In conclusion, it has been demonstrated that a thin bilayer of eC/Au reduces the electron emission order within the multi-photon ionization regime. The presence of sp^2/sp^3 clusters, and the higher confined field in the eC layer facilitates an increased emission at a lower order via the field-driven energy gain. This process allows for electrons to be generated more readily without increasing the laser intensity and thus being limited by the damage threshold. The eC layer was shown to not affect either the SP coupling, or the electromagnetic fields at the Au-vacuum interface, making this a promising candidate for the next generation of ultrafast SP based electron sources driven at low laser intensities.

See [supplementary material](#) for a cartoon sketch of the experimental setup, electric field distributions calculated from FDTD, and simulated exemplary electron trajectories.

This work was supported by the Natural Sciences and Engineering Research Council of Canada (NSERC).

¹S. R. Greig and A. Y. Elezzabi, *Sci. Rep.* **6**, 19056 (2016).

²J. Zawadzka, D. A. Jaroszynski, J. J. Carey, and K. Wynne, *Appl. Phys. Lett.* **79**, 2130 (2001).

³S. E. Irvine, A. Dechant, and A. Y. Elezzabi, *Phys. Rev. Lett.* **93**, 184801 (2004).

⁴S. E. Irvine and A. Y. Elezzabi, *Appl. Phys. Lett.* **86**, 264102 (2005).

⁵P. Dombi, S. E. Irvine, P. Rácz, M. Lenner, N. Kroó, G. Farkas, A. Mitrofanov, A. Baltuška, T. Fuji, F. Krausz, and A. Y. Elezzabi, *Opt. Express* **18**, 24206 (2010).

⁶P. Rácz, S. E. Irvine, M. Lenner, A. Mitrofanov, A. Baltuška, A. Y. Elezzabi, and P. Dombi, *Appl. Phys. Lett.* **98**, 111116 (2011).

⁷P. M. Nagel, J. S. Robinson, B. D. Harteneck, T. Pfeifer, M. J. Abel, J. S. Prell, D. M. Neumark, R. A. Kaindl, and S. R. Leone, *Chem. Phys.* **414**, 106 (2013).

⁸P. Dombi, A. Hörl, P. Rácz, I. Márton, A. Trügler, J. R. Krenn, and U. Hohenester, *Nano Lett.* **13**, 674 (2013).

⁹M. Müller, V. Kravtsov, A. Paarmann, M. B. Raschke, and R. Ernstorfer, *ACS Photonics* **3**, 611 (2016).

¹⁰J. Vogelsang, J. Robin, B. J. Nagy, P. Dombi, D. Rosenkranz, M. Schiek, P. Groß, and C. Lienau, *Nano Lett.* **15**, 4685 (2015).

¹¹J. Kupersztynch, P. Monchicourt, and M. Raynaud, *Phys. Rev. Lett.* **86**, 5180 (2001).

¹²P. Dombi and A. Y. Elezzabi, *Attosecond Nanophysics* (Wiley-VCH Verlag GmbH & Co. KGaA, Weinheim, Germany, 2015), pp. 39–86.

¹³A. Morteza Najarian, B. Szeto, U. M. Tefashe, and R. L. McCreery, *ACS Nano* **10**, 8918 (2016).

- ¹⁴S. M. Sze, *Physics of Semiconductor Devices*, 2nd ed. (Wiley, New York, 1981).
- ¹⁵J. Kupersztych and M. Raynaud, *Phys. Rev. Lett.* **95**, 147401 (2005).
- ¹⁶J. Robertson, *Mater. Sci. Eng., R* **37**, 129 (2002).
- ¹⁷S. Coulombe and J.-L. Meunier, *J. Phys. D: Appl. Phys.* **30**, 776 (1997).
- ¹⁸S. Sederberg and A. Y. Elezzabi, *Phys. Rev. Lett.* **113**, 167401 (2014).
- ¹⁹S. R. Greig and A. Y. Elezzabi, *Appl. Phys. Lett.* **105**, 41115 (2014).
- ²⁰R. L. Olmon, B. Slovick, T. W. Johnson, D. Shelton, S.-H. Oh, G. D. Boreman, and M. B. Raschke, *Phys. Rev. B* **86**, 235147 (2012).
- ²¹J. T. Titantah and D. Lamoen, *Phys. Rev. B* **70**, 33101 (2004).
- ²²J. D. Carey, R. D. Forrest, and S. R. P. Silva, *Appl. Phys. Lett.* **78**, 2339 (2001).
- ²³J. D. Carey, R. D. Forrest, R. U. A. Khan, and S. R. P. Silva, *Appl. Phys. Lett.* **77**, 2006 (2000).
- ²⁴A. Ilie, A. C. Ferrari, T. Yagi, and J. Robertson, *Appl. Phys. Lett.* **76**, 2627 (2000).
- ²⁵N. S. Xu, Y. Tzeng, and R. V. Latham, *J. Phys. D: Appl. Phys.* **26**, 1776 (1993).
- ²⁶H.-S. Hsu, S.-P. Ju, S.-J. Sun, H. Chou, and C. H. Chia, *Europhys. Lett.* **114**, 40001 (2016).